OPF-based Under Frequency Load Shedding Predicting the Dynamic Frequency Trajectory

Quentin Walger, Yihui Zuo, Asja Derviškadić, Guglielmo Frigo, Mario Paolone
Distributed Electrical Systems Laboratory (DESL)
École Polytechnique Fédérale de Lausanne (EPFL)
Lausanne, Switzerland

Abstract—The paper describes a centralized Under Frequency Load Shedding (UFLS) method, where load shedding decisions are based on the solution of an optimization problem. The proposed approach anticipates the evolution of the grid frequency trajectory by means of a system dynamic model. Moreover, the method is augmented by the equations derived from the Optimal Power Flow (OPF) problem allowing to constrain asymptotic values of node voltages and line currents. The proposed OPF-based method differs from traditional UFLS methods as it enables the user to compute the minimum amount of load to be shed and, at the same time, provides a feasible grid trajectory. The trajectory of the system frequency due to the contingency, and the subsequent load shedding, is predicted over the entire time horizon by means of a second-order dynamic model. The feasibility and applicability of the proposed method are assessed by means of numerical simulations carried out using a real-time simulator, where the time-domain full-replica model of the IEEE 39-bus system has been implemented. Two contingency scenarios are investigated and the performance of the proposed method is compared against the UFLS strategy recommended by the European Network of Transmission System Operators (ENTSO-E). The metrics used for such a comparison are the amount of energy not served, the frequency variation and the violation of the grid safety constraints.

Index Terms—Optimal Power Flow, Phasor Measurement Units, Power System Dynamics, Under Frequency Load Shedding

Nomenclature

f	System frequency
$\overline{V}_i, \underline{V}_i, V_i$	Voltage at bus i: complex phasor, conjugate phasor and phasor module
$\overline{I}_{ij}, \underline{I}_{ij}, I_{ij}$	Line current from bus i to bus j: complex phasor, conjugate phasor and phasor module
$\overline{Y}$	System nodal admittance matrix
P_g, Q_g	Active and reactive power of generator g
P_l, Q_l	Active and reactive power of load l
P_{PFR}	Primary frequency regulator power
P_{LoG}	Loss of generation power
H	System total inertia
D	System load damping constant
R_g	Governor droop coefficient of generator g
R_{eq}	Droop coefficient of the equivalent governor
T_{eq}	Time constant of the equivalent governor
S_g	Base power of generator g
S	Base power of the entire system
β	Excitation system characteristic's slope
k_{pv}, k_{pf}	Active power coefficients in load model: voltage exponent and frequency sensitivity
k_{qv}, k_{qf}	Reactive power coefficients in load model: voltage exponent and frequency sensitivity
t_1	Time instant when the contingency occurs
t_2	Time instant when the post-contingency dynamic is exhausted
PMU	Phasor Measurement Unit
T_{PMU}	PMU reporting period
n	Subscript associated to nominal value
LS	Subscript associated to Load Shedding action
min, max	Subscripts associated to minimum and maximum safety values
N, L, G	Total number of buses, loads and generators
i, j, k	Bus indexes defined in the set $[1, \dots N]$
l	Load index defined in the set $[1, \dots L]$
g	Generator index defined in the set $[1, \dots G]$

I. Introduction

Under Frequency Load Shedding (UFLS) is an emergency strategy that minimizes the risk of uncontrolled system separation, loss of generation, or large black-out in case of severe power imbalance [1]. In traditional implementations, the load shedding action depends only on frequency thresholds [2], [3], [4]. Conversely, recent literature has proposed adaptive UFLS methods where the relay considers also the disturbance magnitude [5] or the Rate-of-Change-of-Frequency [6] in order to provide a prompter system reaction.

In general, UFLS methods rely on local control strategies: they do not take into account the state of the entire network, and they set their decision parameters (e.g. frequency thresholds and amount of shed loads) according to standardized guidelines or preliminary calibration stages [7]. However, the single constraint on frequency variation (e.g., in European Continental network between 47.5 and 51.5 Hz [8]) does not prevent from further tripping of lines or generator relays due to the violation of safety limits on node voltages and line/transformers currents. Indeed, a local control relying merely on local information provides a prompt response to

disturbances and faults but is myopic with respect to the overall grid state and cannot determine the optimal load shedding strategy. In this context, the coupling of UFLS with the Optimal Power Flow (OPF) problem represents a promising solution since it can constrain the values of voltages and currents when combined with a model capable to predict the system dynamics [9]. As a matter of fact, centralized decision-making processes relying on a situational awareness system benefit from a system-view enabling the definition of optimal UFLS strategies.

In this paper, we propose an OPF-based UFLS method that not only optimizes the amount of loads to be shed, but also guarantees the non-violation of grid constraints in terms of asymptotic node voltages and line currents. Moreover, a dynamic model of the system frequency response is employed to predict the frequency evolution over the entire time horizon.

The paper is structured as follows. Section II provides a detailed literature review of the state-of-the-art centralized UFLS methods. In Section III, the proposed method is presented. In Section IV, we introduce the network test-bed and the simulated contingency scenarios, and we carry out a thorough performance assessment of the proposed UFLS method in normal and critical conditions. In this context, we compare the proposed UFLS method against the standard approach recommended by the European Network of Transmission System Operators (ENTSO-E). The proposed solution's advantages are quantified in terms of shed load share and in terms of compliance with all the network safety limits. Finally, Section V provides some closing remarks.

II. LITERATURE REVIEW

The power systems literature has widely discussed the UFLS problem and proposed several solutions (e.g. [10]). The traditional approach relies on local frequency measurements and implements a simple logic: once a given threshold is exceeded, a predefined amount of loads is shed in order to preserve grid interconnections and generation capability [2]. As the frequency thresholds are network topology- and state-dependent, their setting is typically carried out by means of simulation-based trial-and-error heuristics [11]. However, this approach neglects the dynamic contingency response, and approximates the network via a purely static model [12].

In this context, Phasor Measurement Units (PMUs) provide an effective tool to track the network state in any node of interest with reporting rates in the order of tens of frames per seconds. The availability of such distributed measurement infrastructure has triggered the development of more sophisticated local [6] and centralized UFLS methods [13] that exploit the frequency and ROCOF information. In this regard, ROCOF-based relays have shown to provide a prompter and more effective response thanks to the anticipative effect inherent in their time-derivative formulation [14].

However, in the presence of high shares of distributed generation, UFLS methods might produce unnecessary load disconnections and thus lead to frequency instability [15], [16], [17]. In order to overcome this limitation, UFLS methods are

formulated as optimization problems that minimize the expected amount of shed loads, taking into account the dynamic system frequency response [18], as well as the unnecessary activation of protection relays [19]. A multi-objective mixed-integer linear program is proposed in [20] to minimize the load shedding amount and voltage deviation simultaneously.

In [9], a unified control framework allows to manage not only frequency but also the power imbalance. More specifically, by including the OPF equations within the optimization problem constraints, it is possible to restore the nominal frequency, maintaining nodal voltages, line currents and power flows within the safety limits. In line with this approach, the present paper adopts similar OPF constraints and applies them to an UFLS method that not only optimizes the amount of loads to be shed, but also considers the dynamic response of the network in order not to exceed any safety constraint.

III. THE PROPOSED METHOD

The proposed method is meant to enhance the performance of emergency operational practices in Transmission System Operator (TSO) control rooms. The method leverages on the real-time situational awareness provided by a Supervisory Control And Data Acquisition (SCADA) system fed by time-stamped synchrophasor measurements. It is reasonable to assume that the network model, combining network topology and electrical parameters of the network components, is assessed in real-time in the TSO control room. The topology can be indeed constructed by collecting the breaker/switch statuses that are streamed by PMUs [21]. This includes any loss of generation that might call for UFLS action. The parameters of the network components, instead, are usually well-known by the TSO. Based on the network model and on the gathered synchrophasors, the system state can be estimated in real-time with time delays in the order of 100 ms [22]. Based on the results of the state estimation process, the proposed UFLS method runs in parallel to conventional contingency analysis. This centralized approach, besides benefiting of a wide-area vision of the system state, can be easily coupled with other emergency control and protection operation and management actions. It is worth to point out that the proposed method could also rely on conventional measurements provided by remote terminal units (RTU) in substations, as long as a reliable and accurate estimation of the system state is provided in real-time.

Working hypothesis: The proposed method is based on the following hypothesis:

1) The nodal admittance matrix $\overline{Y}$, network topology and parameters are known in real-time.
2) The system state is tracked in real-time by means of PMUs feeding a suitable state estimation process, guaranteeing the full observability of the system state [23].
3) The controlled variables are the average system frequency f, the node voltage phasors $\overline{V}_i$ and the line current phasors $\overline{I}_{ij}$ as provided by the PMU-fed state estimator.
4) The control variables are the loads to be shed in terms of active power $\Delta P_{l,LS}$ in each load bus l.

Problem formulation: The amount of loads to be shed is determined by solving the following optimization problem. Each constraint is discussed in details in the following sections, including the simplifications introduced in order to achieve a convex and tractable formulation.

$$\min_{\Delta P_{l,LS}} \sum_{l=1}^{L} \Delta P_{l,LS} \qquad (1)$$

subject to:

$$\begin{cases} f_{min}^{t\in[t_1,t_2]} \le f(t) \le f_{max}^{t\in[t_1,t_2]} & \forall t \in [t_1,t_2] \\ f_{min}^{t\to\infty} \le f(t) \le f_{max}^{t\to\infty} & t \to \infty \end{cases} \qquad (2)$$

$$V_{i,min} \le V_i \le V_{i,max} \qquad (3)$$

$$I_{ij} \le I_{ij,max} \qquad (4)$$

$$\begin{cases} \frac{d\Delta f(t)}{dt} = \frac{f_n}{2H}\Big(\Delta P_{PFR}(t) - P_{LoG} + \\ \qquad + \sum \Delta P_{l,LS} - D\Delta f(t) \Big) \\ \frac{d\Delta P_{PFR}(t)}{dt} = -\frac{1}{T_{eq}}\Big(\Delta P_{PFR}(t) + \frac{\Delta f(t)}{R_{eq}} \Big) \end{cases} \qquad (5)$$

$$\Delta P_g = \begin{cases} -\frac{1}{R_g}\Delta f & \text{if } -\frac{1}{R_g}\Delta f \le \Delta P_{g,max} \\ \Delta P_{g,max} & \text{if } -\frac{1}{R_g}\Delta f > \Delta P_{g,max} \end{cases} \qquad (6)$$

$$\Delta Q_g = \begin{cases} \beta\Delta P_g & \text{if } V_g > \frac{Q_g - \beta P_g}{Q_{P=0}} \\ \frac{Q_{g,n}}{P_{g,n}}\Delta P_g & \text{if } V_g \le \frac{Q_g - \beta P_g}{Q_{P=0}} \end{cases} \qquad (7)$$

$$\Delta P_l = \Delta P_{l,LS} + \frac{P_{l,n}k_{pv}}{V_n}\Delta V_l + P_{l,n}k_{pf}\Delta f \qquad (8)$$

$$0 \le \Delta P_{l,LS} \le 0.5|P_{l,n}| \qquad (9)$$

$$\Delta Q_l = \Delta Q_{l,LS} + \frac{Q_{l,n}k_{qv}}{V_n}\Delta V_l + Q_{l,n}k_{qf}\Delta f \qquad (10)$$

$$\Delta Q_{l,LS} = \Delta P_{l,LS}\frac{Q_{l,n}}{P_{l,n}} \qquad (11)$$

$$\Delta\overline{V}_i \cong \frac{\partial\overline{V}_i}{\partial P_k}\Delta P_k + \frac{\partial\overline{V}_i}{\partial Q_k}\Delta Q_k - \frac{\partial\overline{V}_i}{\partial|\overline{V}_g|}|\Delta\overline{V}_g| \qquad (12)$$

$$\Delta\overline{I}_{ij} \cong \frac{\partial\overline{I}_{ij}}{\partial P_k}\Delta P_k + \frac{\partial\overline{I}_{ij}}{\partial Q_k}\Delta Q_k - \frac{\partial\overline{I}_{ij}}{\partial|\overline{V}_g|}|\Delta\overline{V}_g| \qquad (13)$$

A. Grid Constraints

In order not to violate frequency, current and voltage limits, the proposed method applies the following grid constraints:

$$\begin{cases} f_{min}^{t\in[t_1,t_2]} \le f(t) \le f_{max}^{t\in[t_1,t_2]} & \forall t \in [t_1,t_2] \\ f_{min}^{t\to\infty} \le f(t) \le f_{max}^{t\to\infty} & t \to \infty \end{cases} \qquad (14)$$

$$V_{i,min} \le V_i \le V_{i,max} \qquad (15)$$

$$I_{ij} \le I_{ij,max} \qquad (16)$$

In particular, as defined in grid codes (e.g., [8], [24]), the system frequency should be kept within the ordinary operation range during close-to-static operating conditions. Following large contingencies, instead, these limits are relaxed allowing for an initial frequency transient, that, depending on the contingency severity, can last for tens of seconds. In the Continental Europe synchronous area, the primary control reserves are designed to limit the system frequency variations within the

range between 49.8 and 50.2 Hz. The emergency operation range, i.e., during the time range $[t_1, \dots t_2]$, is defined within 47.5 and 51.5 Hz: if the frequency exceeds such range, it is hard to avoid a system blackout [8].

As regards the voltage, the safety constraints are set to $\pm10\%$ of the rated voltage as defined in grid codes (e.g., [25], [26]). The limit on the currents is set as the maximum capacity of each transmission line, that depends on the line physical and geometric characteristics.

B. System Frequency Response

After a generic contingency, the proposed method predicts the frequency trajectory due to the power imbalance and to the subsequent load shedding by means of an equivalent frequency dynamic response model. In particular, the method assumes that all generators within the same area swing synchronously at a common frequency f. Hence, the system frequency response for the considered area is obtained through an equivalent single-machine swing equation, inversely proportional to the overall system inertia [27]:

$$\frac{d\Delta f(t)}{dt} = \frac{f_n}{2H}\Big(\Delta P_{PFR}(t) - P_{LoG} + \qquad (17)$$
$$+ \sum \Delta P_{l,LS} - D\Delta f(t) \Big)$$

where $\Delta f(t)$ refers to the system frequency deviation from the nominal frequency f_n following the loss of generation P_{LoG}, H is the total inertia of the system, $\sum \Delta P_{l,LS}$ is the cumulative amount of shed loads, D is the system load damping constant, and ΔP_{PFR} is the power deviation due to the equivalent primary frequency regulator.

The system primary frequency regulation is represented as a first-order differential equation:

$$\frac{d\Delta P_{PFR}(t)}{dt} = -\frac{1}{T_{eq}}\Big(\Delta P_{PFR}(t) + \frac{\Delta f(t)}{R_{eq}} \Big) \qquad (18)$$

where R_{eq} is the equivalent governor droop coefficient and T_{eq} is the time constant related to the equivalent governor action.

The equivalent governor droop R_{eq} is derived from the individual generator droops R_g:

$$\frac{1}{R_{eq}} = \sum_{g=1}^{G} \frac{S_g}{SR_g} \qquad (19)$$

where S_g is the power base of generator g and S is the system power base. In order to infer the values of the system load damping D and of the governor time constant T_{eq} a sensitivity analysis is carried out by considering different disturbances within the considered grid. In particular, a curve fitting tool determines T_{eq} and D that suitably describe the system frequency response in terms of single-machine swing equation (17) and equivalent primary frequency regulator (18).

C. Generators

As regards the generators, their active power is determined based on the generator's droop characteristic:

$$\Delta P_g = \begin{cases} -\frac{1}{R_g}\Delta f & \text{if } -\frac{1}{R_g}\Delta f \leq \Delta P_{g,max} \\ \Delta P_{g,max} & \text{if } -\frac{1}{R_g}\Delta f > \Delta P_{g,max} \end{cases} \quad (20)$$

In particular, as long as the computed active power deviation ΔP_g is lower than the maximum attainable power output, the droop characteristic is considered. Otherwise, the power is set to the generator's maximum set-point. The reactive power, instead, is computed as a function of the active power, scaled to a voltage-dependent factor:

$$\Delta Q_g = \begin{cases} \beta \Delta P_g & \text{if } V_g > \frac{Q_g - \beta P_g}{Q_{P=0}} \\ \frac{Q_{g,n}}{P_{g,n}}\Delta P_g & \text{if } V_g \leq \frac{Q_g - \beta P_g}{Q_{P=0}} \end{cases} \quad (21)$$

where $Q_{P=0}$ is the reactive power absorbed by the generator in case of null supplied active power and β is the inverse of the under-excitation characteristic's slope. In particular, the synchronous generators embed the excitation system presented in Fig. 1. Based on such scheme, and as presented in (21), the reactive power deviation ΔQ_g depends on the voltage at the generator's output V_g. Specifically, in case V_g exceeds a specific threshold, ΔQ_g is proportional to β. For V_g below the threshold, ΔQ_g is proportional to ΔP_g.

D. Loads

The proposed method relies on the Electric Power Research Institute (EPRI) LOADSYN model [28], that is adaptable to different systems and conditions and is recommended for large-scale transient stability simulations [29]. In particular, the loads are modeled as follows:

$$P_l = (P_{l,n} + \Delta P_{l,LS})\left(\frac{V_l}{V_n}\right)^{k_{pv}}(1 + k_{pf}(f_l - f_n)) \quad (22)$$

$$Q_l = (Q_{l,n} + \Delta Q_{l,LS})\left(\frac{V_l}{V_n}\right)^{k_{qv}}(1 + k_{qf}(f_l - f_n)) \quad (23)$$

where $P_{l,n}$ and $Q_{l,n}$ represent the power consumed at the rated voltage and system frequency and $\Delta P_{l,LS}$ and $\Delta Q_{l,LS}$ are the amount of shed power at load l. As regards the load voltage and frequency parameters $k_{pv}, k_{pf}, k_{qv}, k_{qf}$, [28] provides a comprehensive set of empirically determined parameters for various load classes.

In order to achieve a convex formulation, these load equations are linearized around the pre-contingency active and reactive power set-points:

$$\Delta P_l = \Delta P_{l,LS} + \frac{P_{l,n}k_{pv}}{V_n}\Delta V_l + P_{l,n}k_{pf}\Delta f \quad (24)$$

$$\Delta Q_l = \Delta Q_{l,LS} + \frac{Q_{l,n}k_{qv}}{V_n}\Delta V_l + Q_{l,n}k_{qf}\Delta f \quad (25)$$

To estimate the shed reactive power, we assume that the $\cos\phi$ of the loads remains constant, i.e., the ratio between reactive and active power is assumed to remain constant:

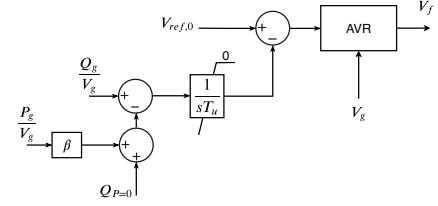$$\Delta Q_{l,LS} = \Delta P_{l,LS}\frac{Q_{l,n}}{P_{l,n}} \quad (26)$$

Fig. 1: Diagram of the excitation system accounting for active and reactive power: $V_{ref,0}$ is the generator nominal voltage, T_u the under-excitation time constant, V_f the excitation voltage.

In addition, as recommended by traditional UFLS methods (e.g., [2]), the amount of load shedding is limited to 50 % of the rated load power:

$$0 \leq \Delta P_{l,LS} \leq 0.5\,|P_{l,n}| \quad (27)$$

E. Node Voltages and Line Currents

The proposed method determines the node voltages $\overline{V}_i$ and line currents $\overline{I}_{ij}$ as a linearized function of the nodal power injections, using the sensitivity coefficients introduced in [30]. To derive the voltage sensitivity coefficients, the partial derivatives of voltage $\overline{V}_i$ with respect to the active and reactive power P_k and Q_k of a bus $k \in [1, ..., N]$ have to be computed, as well as the partial derivatives of the voltage with respect to the generators voltage magnitude V_g ($g \in [1, ..., G]$):

$$\mathbb{1}_{\{i=k\}} = \frac{\partial \underline{V}_i}{\partial P_k}\sum_{j=1}^{N}\overline{Y}_{ij}\overline{V}_j + \underline{V}_i\sum_{j=1}^{N}\overline{Y}_{ij}\frac{\partial \overline{V}_j}{\partial P_k} \quad (28)$$

$$-\mathbb{1}_{\{i=k\}} = \frac{\partial \underline{V}_i}{\partial Q_k}\sum_{j=1}^{N}\overline{Y}_{ij}\overline{V}_j + \underline{V}_i\sum_{j=1}^{N}\overline{Y}_{ij}\frac{\partial \overline{V}_j}{\partial Q_k} \quad (29)$$

$$0 = \frac{\partial \underline{V}_i}{\partial |\overline{V}_g|}\sum_{j=1}^{N}\overline{Y}_{ij}\overline{V}_j + \underline{V}_i\sum_{j=1}^{N}\overline{Y}_{ij}\frac{\partial \overline{V}_j}{\partial |\overline{V}_g|} \quad (30)$$

It is worth pointing out that this linear system of equations enables us to compute the sensitivity coefficients associated to voltage and current by knowing only the system state. In particular, the partial derivatives of the magnitude of the voltage at bus i with respect to active and reactive power at bus k and with respect to voltage magnitude of generator g are defined as:

$$\frac{\partial |\overline{V}_i|}{\partial P_k} = \frac{1}{|\overline{V}_i|}\operatorname{Re}\left\{\underline{V}_i\frac{\partial \overline{V}_i}{\partial P_k}\right\} \quad (31)$$

$$\frac{\partial |\overline{V}_i|}{\partial Q_k} = \frac{1}{|\overline{V}_i|}\operatorname{Re}\left\{\underline{V}_i\frac{\partial \overline{V}_i}{\partial Q_k}\right\} \quad (32)$$

$$\frac{\partial |\overline{V}_i|}{\partial |\overline{V}_g|} = \frac{1}{|\overline{V}_i|}\operatorname{Re}\left\{\underline{V}_i\frac{\partial \overline{V}_i}{\partial |\overline{V}_g|}\right\} \quad (33)$$

Based on these sensitivity coefficients, it is possible to approximate voltage variations as linearized functions of active, reactive power and generators voltage magnitude variations:

$$|\Delta \overline{V}_i| \cong \frac{\partial |\overline{V}_i|}{\partial P_k}\Delta P_k + \frac{\partial |\overline{V}_i|}{\partial Q_k}\Delta Q_k - \frac{\partial |\overline{V}_i|}{\partial |\overline{V}_g|}|\Delta \overline{V}_g| \quad (34)$$

The voltage variation $\Delta\overline{V}_g$ in generator g is computed as the pre-contingency difference between the generator's voltage and the voltage of its upstream bus (i.e., secondary side of its transformer). This formulation enables taking into account the change of topology induced by the tripping of the generator. It should be pointed out that $\Delta\overline{V}_g$ is 0 in generators that are not tripped, since no change of topology occurs in those locations.

The variation of the currents magnitude could be estimated in a similar way as (34), however, it becomes problematic in case $\Delta I_{ij} < -|\overline{I}_{ij,0}|$ (with $\overline{I}_{ij,0}$ being the pre-contingency current in line ij) since this would yield a negative magnitude. Instead, we propose to compute the magnitude of the current based on its real and imaginary components:

$$\Delta\overline{I}_{ij} \cong \frac{\partial\overline{I}_{ij}}{\partial P_k}\Delta P_k + \frac{\partial\overline{I}_{ij}}{\partial Q_k}\Delta Q_k - \frac{\partial\overline{I}_{ij}}{\partial|\overline{V}_g|}|\Delta\overline{V}_g| \qquad (35)$$

$$|\overline{I}_{ij}| = \sqrt{\mathrm{Re}\left\{\overline{I}_{ij,0} + \Delta\overline{I}_{ij}\right\}^2 + \mathrm{Im}\left\{\overline{I}_{ij,0} + \Delta\overline{I}_{ij}\right\}^2} \qquad (36)$$

Constraint (36) is a nonlinear, hence non-convex equality constraint. However, it is not included, as is, in the optimization problem, since it is injected into (4) which then becomes a nonlinear, but convex inequality constraint. To achieve a linear formulation, the ampacity circle can be piecewise linearized, yielding a set of linear constraints.

F. Computational Complexity

The problem formulation as presented so far, could be solved at every time-step, thus leading to very accurate predictions of all the controlled (system frequency, voltage and current phasors) and control (power injections) variables. However, the computational complexity associated to solving the whole problem of equations (1)-(13), is too demanding, even though all expressions have been properly linearized. In particular, as discussed in Section III-D, the piecewise linearization of the load models in (24) and (25) involves three decision variables (amount of shed power, voltage magnitude and frequency). This results in multivariate (three-dimensional) constraints, therefore leading to an intractable optimization problem.

Also, as described in Section III-E, (28) to (30), the computation of the sensitivity coefficients implies solving a linear system of equations, in which the matrix to be inverted changes over time based on the decision variables of the previous time-step, that is computationally demanding. In view of reducing the computational complexity of the proposed method, only the trajectory of the frequency is predicted over the entire time-horizon, according to (17) and (18). As regards the remaining variables, i.e., the bus voltages, the line currents, and the bus active and reactive power profiles (for both generation and load buses), only their asymptotic value is computed:

$$\Delta V_i(t), \Delta I_{ij}(t), \Delta P_i(t), \Delta Q_i(t) \qquad \text{only for } t \to \infty \qquad (37)$$

$$f(t) \qquad \forall t \qquad (38)$$

Nevertheless, it should be noticed that the proposed method is scalable, since each synchronous generator can be regarded
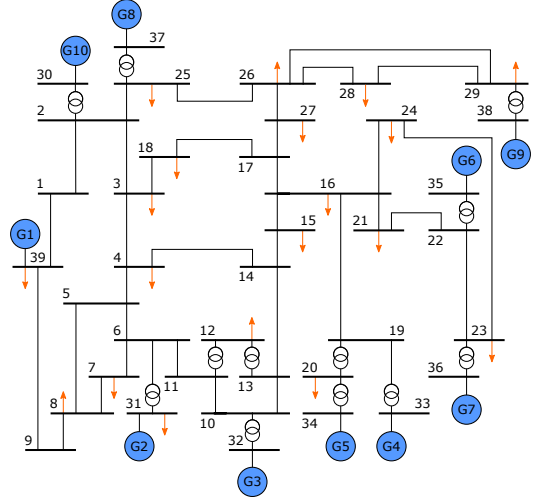

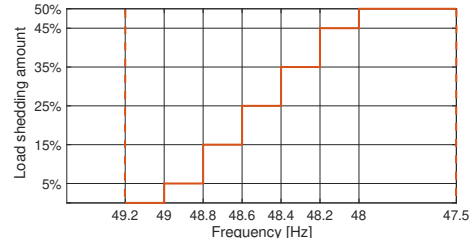Fig. 2: Scheme of the IEEE 39-bus power grid Opal-RT simulation model [31].

Fig. 3: ENTSO-E recommendation for frequency threshold settings in standard UFLS relays [2].

as the dynamic equivalent model of a synchronous area. Furthermore, for the sake of generality, each area could be characterized by a specific system frequency response model.

In order to give a quantitative evaluation of the overall computational complexity, given a network model with N nodes and a prediction horizon of M time steps, the worst-case complexity is $O(N^2 + NM)$ in terms of both decision variables and constraints.

IV. PERFORMANCE ASSESSMENT

In order to assess the performance of the proposed technique over large-scale power systems, the Opal-RT eMEGAsim PowerGrid Real Time Simulator (RTS) is used to implement a detailed dynamic model of the IEEE 39-bus power system, also known as 10-machine New-England power system (see Fig. 2) [32]. This model represents a widely-employed benchmark for performance evaluation and comparison of power system operation and management practices. In more detail, the simulated power system consists in 39 buses (10 generators and 19 loads) and is characterized by a nominal voltage of 345 kV. In order to emulate realistic load patterns, load profiles are adapted from real measurements. The model is available online [31] and thorough details are provided in [33].

The electrical grid is fully equipped with simulated PMUs, embedding the e-IpDFT synchrophasor estimator for P-class of

TABLE I: Load buses: load coefficients and pre-contingency power injections

Load #	1	2	3	4	5	6	7	8	9	10	11	12	13	14	15	16	17	18	19
Bus #	3	4	7	8	12	15	16	18	20	21	23	24	25	26	27	28	29	31	39
k_{pv}	1.7	0.5	0.6	1.7	1.5	1.7	1.6	1.5	0.7	1.7	1.5	0.8	1.5	1.6	0.6	0.5	0.7	1.7	1.1
k_{qv}	2.5	2.5	2.5	2.6	2.5	2.5	3.1	2.8	2.5	2.6	3	2.4	2.5	2.9	2.5	2.5	2.5	2.6	2.6
k_{pf}	1	1.2	1.5	1	0.9	1	0.7	0.9	1.3	1	0.8	1.7	0.9	0.8	1.5	1.2	1.3	1	0.8
k_{qf}	-1.5	-1.6	-1.1	-1.7	-1.8	-1.5	-1.9	-1.3	-1.9	-1.7	-1.7	-0.9	-1.8	-1.6	-1.1	-1.6	-1.9	-1.7	-2.3
P [MW]	322	500	233	522	13	320	329	158	633	274	274	308	224	139	281	206	283	8	1104
Q [MVAR]	2	184	84	176	88	153	32	30	103	115	85	-92	47	17	75	28	27	4	250

TABLE II: Generation buses: pre-contingency set-points

Gen #	1	2	3	4	5	6	7	8	9	10
Bus #	39	31	32	33	34	35	36	37	38	30
P [MW]	1129	526	692	638	511	657	605	547	837	301
Q [MVAR]	411	257	270	151	177	222	45	-74	30	151

TABLE III: Expected Energy Not Served

	Standard UFLS	OPF-UFLS Scenario 1
EENS [MWh]	10.9	4.3

performance [34]. The virtual PMUs are installed at each bus and are characterized by sampling and reporting rate equal to 10 kHz and 50 frames per second, respectively. They measure the bus voltage and line current synchrophasors, as well as frequency and ROCOF. These measurements are sent to the UFLS controller, that acts on the demand profile based on the UFLS strategy. Since the formulation of a state estimator is out of the scope of this paper, and since in a simulated environment, we can equip every node with a PMU we directly feed PMU measurements in the optimization problem.

For comparison purposes, the results are compared with those obtained in case of utilizing the UFLS strategy recommended by the ENTSO-E [2]. Specifically, the ENTSO-E recommends a local control scheme, hereafter referred to as *Standard UFLS*, according to which loads are shed proportionally to the measured frequency deviation. Fig. 3 shows the recommended frequency thresholds as well as the corresponding load shedding amount.

We carry out dedicated simulations in case of tripping generators Gen 5 and Gen 6 and we consider two scenarios: *Scenario 1* and *Scenario 2*. The results for *Scenario 1* are presented in Section IV-A for a power system operating in close-to-nominal conditions and in Section IV-B for a power system operating in heavily loaded conditions, with the pre-contingency line currents of lines 2-3 and 13-14 close to their respective ampacity limit. The results for *Scenario 2* are intended to verify whether the proposed UFLS approach is able to maintain node voltages and line currents within the grid safety constraints.

A. Scenario 1

In *Scenario 1*, the power system is operating in close-to-nominal conditions, i.e., no generator is close to its maximum power output and no node voltage or line current is close to its

corresponding limit. The pre-contingency power injections are shown in Table I and Table II. The output power of generators Gen 5 and Gen 6 are tripped at 180 s, yielding a loss of generation of 1100 MW. We assume here that the frequency should not drop below 49 Hz, that is $f_{min}^{t \in [t_1, t_2]} = 49\ Hz$.

Fig. 4 shows the evolution of frequency, bus active power, node voltage and line current for the proposed OPF-based UFLS. The curves referred as *True* are the simulation results obtained by the application of the proposed UFLS, while the curves referred as *Pred* are the predicted values. The curves referred as *Standard UFLS* are the simulation results relative to the application of the standard UFLS scheme. Note that the predicted values are presented over the entire time horizon for the frequency, and just as asymptotic values for power profiles, node voltages and line currents.

All the states are correctly predicted, allowing to keep the frequency above 49 Hz during the transient following the contingency and 49.5 Hz in the subsequent steady-state. More specifically, Fig. 4(a) shows the frequency response of generator Gen 1 for both OPF-based UFLS and the standard UFLS approaches. Moreover, Fig. 4(b) refers to the power profiles in three loads for the proposed OPF-based UFLS, showing that in order to counteract the contingency 46 % of Load 12 (143 MW) is shed. Conversely, the standard UFLS sheds 367 MW in total.

Table III presents the results in terms of expected energy not served (EENS), defined as the expected amount of energy not being served to the demand during the UFLS action. The EENS is calculated for a time period of 110 seconds after the load shedding, for both the OPF-based UFLS and the standard UFLS. In Scenario 1, the amount of EENS for the standard UFLS is more than twice the one for the OPF-based UFLS.

B. Scenario 2

In *Scenario 2*, the pre-contingency power injections (i.e., values as in Table I and Table II) and the loss of generation (1100 MW) are the same as in *Scenario 1*. Conversely, we reduce the ampacity of lines 2-3 (index 3) and 13-14 (index 20) close to their respective pre-contingency line currents. In particular, the pre-contingency line currents are 3.72 pu in line 2-3 and 3.07 pu in line 13-14. We set the ampacity of line 2-3 to 4.5 pu and of line 13-14 to 4 pu. Therefore, although the loss of generation is the same as in *Scenario 1*, a different load shedding strategy is required in order to meet the ampacity constraints on lines 2-3 and 13-14. By contrast, the standard UFLS produces exactly the same results.
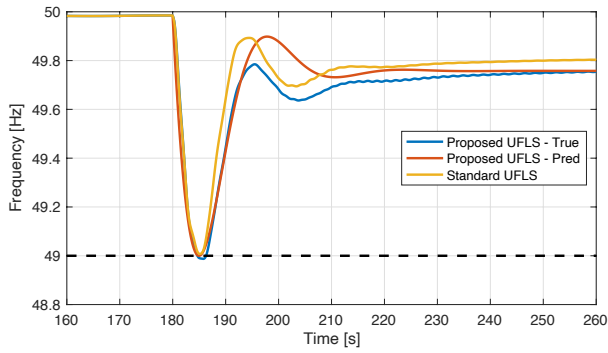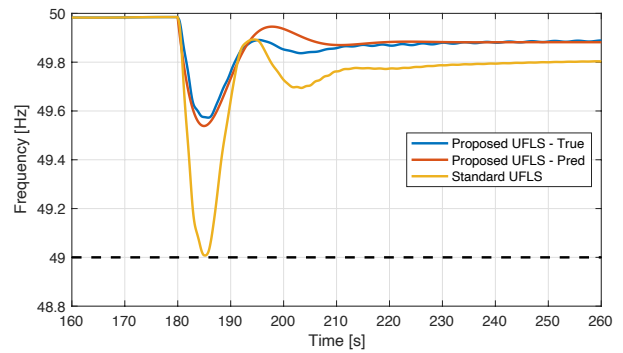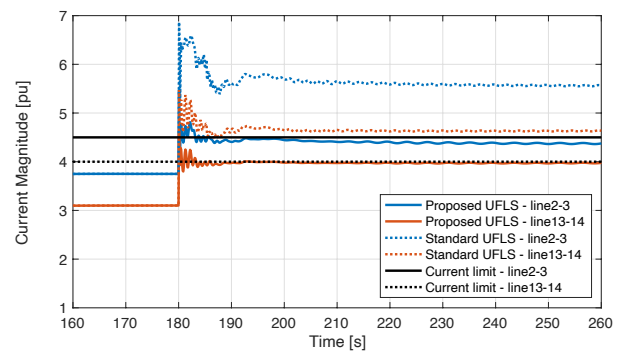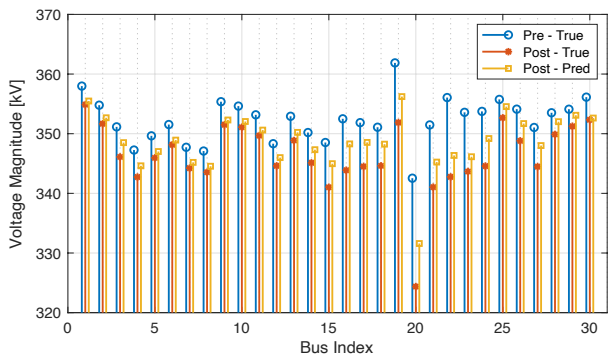
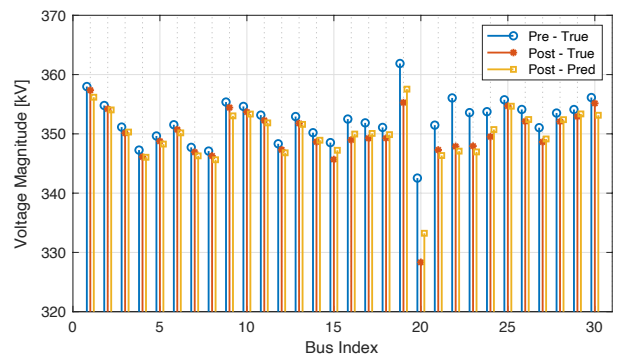(a) Frequency of generator 1: proposed UFLS true (blue) and predicted (red) values; standard UFLS (yellow).
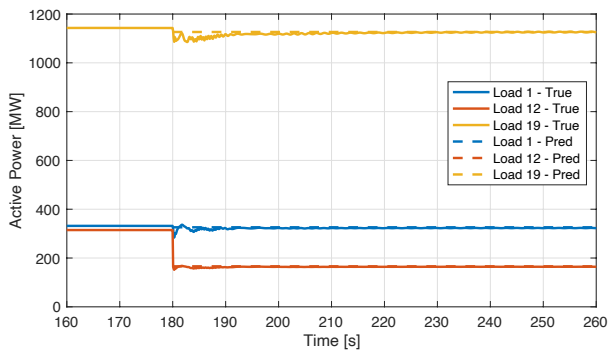
(b) Active power profiles: load 1 (blue), 12 (red) and 19 (yellow); true (solid line) and predicted (dashed line) values.

(c) Voltage profile in all buses: pre-contingency (blue) and post-contingency true (red) and predicted (yellow) values.

(d) Current flow in all lines: pre-contingency (blue) and post-contingency true (red) and predicted (yellow) values.

Fig. 4: Results *Scenario 1*.

(a) Frequency of generator 1: proposed UFLS true (blue) and predicted (red) values; standard UFLS (yellow).
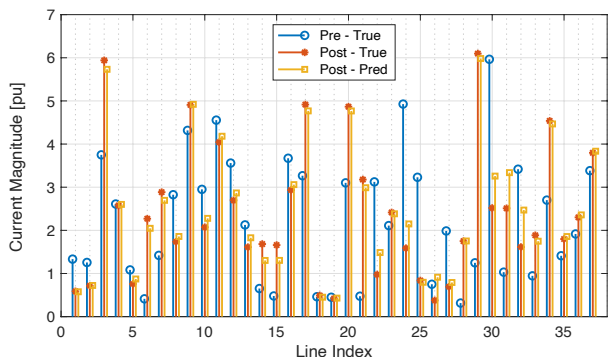

(b) Current capacity: proposed (solid line) and standard (dotted line) UFLS results in line 2-3 (blue) and line 13-14 (red).

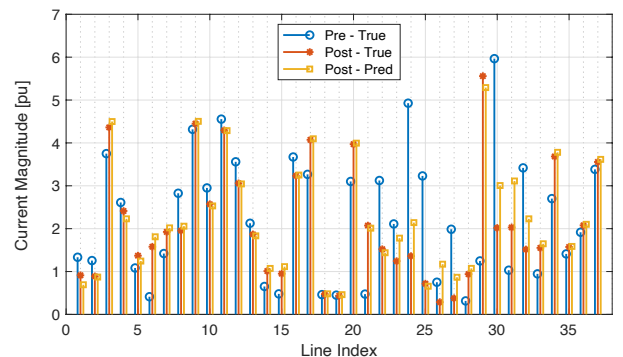(c) Voltage profile in all buses: pre-contingency (blue) and post-contingency true (red) and predicted (yellow) values.

(d) Current flow in all lines: pre-contingency (blue) and post-contingency true (red) and predicted (yellow) values.

Fig. 5: Results *Scenario 2*.

Fig. 5 presents the simulation results for frequency, node voltages and line currents. As shown in Fig. 5(a), a higher amount of load shedding is required to meet the ampacity constraints, causing the drop of the frequency to be smaller. In particular, the load shedding is now distributed among several loads, for a total amount of 703 MW. Finally, Fig. 5(b) demonstrates that the proposed OPF-based UFLS enables us to respect the ampacity limits of lines 2-3 and 13-14. The standard UFLS, instead, violates such limits leading to a current of 5.5 pu in line 2-3 and 4.6 pu in line 13-14.

V. CONCLUSIONS

The paper describes a centralized UFLS scheme based on an optimization problem whose constraints include grid constraints, a dynamic model of the frequency, power flow equations and a model for voltage- and frequency-dependent loads. The proposed approach is different from traditional UFLS schemes in the sense that the evolution of the states that follows the load shedding is anticipated. This allows, in addition to controlling the trajectory of the frequency, to ensure that voltages and currents do not violate their safety limits.

Two contingency scenarios were investigated by means of real-time simulation over a full replica model of the IEEE 39-bus power system. The results show that the proposed UFLS scheme outperforms the traditional ENTSO-E approach, in terms of EENS and grid constraints compliance.

REFERENCES

[1] "IEEE guide for the application of protective relays used for abnormal frequency load shedding and restoration," *IEEE Std C37.117-2007*, pp. 1–55, Aug 2007.

[2] ENTSO-E, "Technical background and recommendations for defence plans in the continental Europe synchronous area," European Network of Transmission System Operators for Electricity, Tech. Rep., 2010.

[3] U. Rudez and R. Mihalic, "Analysis of underfrequency load shedding using a frequency gradient," *IEEE Transactions on Power Delivery*, vol. 26, no. 2, pp. 565–575, April 2011.

[4] NERC, "Automatic underfrequency load shedding," *NERC Std PRC-006-3, North American Electric Reliability Corporation*, 2017.

[5] J. Tang, J. Liu, F. Ponci, and A. Monti, "Adaptive load shedding based on combined frequency and voltage stability assessment using synchrophasor measurements," *IEEE Transactions on Power Systems*, vol. 28, no. 2, pp. 2035–2047, May 2013.

[6] Y. Zuo, G. Frigo, A. Derviškadić, and M. Paolone, "Impact of synchrophasor estimation algorithms in ROCOF-based under-frequency load-shedding," *IEEE Transactions on Power Systems*, pp. 1–1, 2019.

[7] V. Terzija, "Adaptive underfrequency load shedding based on the magnitude of the disturbance estimation," *IEEE Transactions on Power Systems*, vol. 21, no. 3, pp. 1260–1266, Aug 2006.

[8] ENTSO-E, "Frequency stability evaluation criteria for the synchronous zone of continental Europe," European Network of Transmission System Operators for Electricity, Tech. Rep., 2016.

[9] C. Zhao, E. Mallada, S. Low, and J. Bialek, "A unified framework for frequency control and congestion management," in *2016 Power Systems Computation Conference (PSCC)*, June 2016, pp. 1–7.

[10] B. Delfino, S. Massucco, A. Morini, P. Scalera, and F. Silvestro, "Implementation and comparison of different under frequency load-shedding schemes," in *2001 Power Engineering Society Summer Meeting*, vol. 1, July 2001, pp. 307–312 vol.1.

[11] J. R. Jones and W. D. Kirkland, "Computer algorithm for selection of frequency relays for load shedding," *IEEE Computer Applications in Power*, vol. 1, no. 1, pp. 21–25, Jan 1988.

[12] F. Ceja-Gomez, S. S. Qadri, and F. D. Galiana, "Under-frequency load shedding via integer programming," *IEEE Transactions on Power Systems*, vol. 27, no. 3, pp. 1387–1394, Aug 2012.

[13] M. Karimi, P. Wall, H. Mokhlis, and V. Terzija, "A new centralized adaptive underfrequency load shedding controller for microgrids based on a distribution state estimator," *IEEE Transactions on Power Delivery*, vol. 32, no. 1, pp. 370–380, Feb 2017.

[14] G. Frigo, A. Derviškadić, Y. Zuo, and M. Paolone, "PMU-based ROCOF measurements: Uncertainty limits and metrological significance in power system applications," *IEEE Transactions on Instrumentation and Measurement*, pp. 1–1, 2019.

[15] K. Das, A. Nitsas, M. Altin, A. D. Hansen, and P. E. Sørensen, "Improved load-shedding scheme considering distributed generation," *IEEE Transactions on Power Delivery*, vol. 32, no. 1, pp. 515–524, Feb 2017.

[16] E. Mallada, C. Zhao, and S. Low, "Optimal load-side control for frequency regulation in smart grids," *IEEE Transactions on Automatic Control*, vol. 62, no. 12, pp. 6294–6309, Dec 2017.

[17] AEMO, "Black System South Australia 28 September 2016," Australian Energy Market Operator, Tech. Rep., 2017.

[18] M. Ghaderi Darebaghi and T. Amraee, "Dynamic multi-stage under frequency load shedding considering uncertainty of generation loss," *IET Generation, Transmission Distribution*, vol. 11, no. 13, pp. 3202–3209, 2017.

[19] T. Amraee, M. G. Darebaghi, A. Soroudi, and A. Keane, "Probabilistic under frequency load shedding considering RoCoF relays of distributed generators," *IEEE Transactions on Power Systems*, vol. 33, no. 4, pp. 3587–3598, July 2018.

[20] M. Alizadeh, M. Jafari-Nokandi, and T. Amraee, "Multiobjective optimal setting for UFLS relays considering voltage deviation," *International Transactions on Electrical Energy Systems*, vol. 29, no. 3, 2019.

[21] L. Zanni, A. Derviškadić, M. Pignati, C. Xu, P. Romano, R. Cherkaoui, A. Abur, and M. Paolone, "PMU-based linear state estimation of Lausanne subtransmission network: Experimental validation," *Electric Power Systems Research (EPSR), special issue of the 2020 Power Systems Computation Conference (PSCC)*, pp. 1–7, June 2020.

[22] A. Derviškadić, P. Romano, M. Pignati, and M. Paolone, "Architecture and experimental validation of a low-latency phasor data concentrator," *IEEE Transactions on Smart Grid*, vol. 9, no. 4, pp. 2885–2893, July 2018.

[23] M. Paolone, J.-Y. L. Boudec, S. Sarri, and L. Zanni, *Advances in Power System Modelling, Control and Stability Analysis*. F. Milano, Ed. Edison, NJ, USA: IET, 2015, ch. 6: Static and recursive PMU-based state estimation processes for transmission and distribution power grids.

[24] AEMC, "Application of frequency operating standards during periods of supply scarcity," Reliability Panel of the Australian Energy Market Commission, Tech. Rep., 2009.

[25] IEC, "International Standard 60038 standard voltages," *IEC 60038:2009*, pp. 1–26, June 2009.

[26] CEI, "EN 50160 Voltage characteristics of electricity supplied by public electricity networks," *EN 50160:2010/A1:2015*, pp. 1–14, Sept. 2015.

[27] F. Saccomanno, *Electric Power Systems: Analysis and Control*. Wiley-IEEE Press, 2003, ch. 4: Dynamic Behavior of the Synchronous Machine.

[28] "Load representation for dynamic performance analysis (of power systems)," *IEEE Transactions on Power Systems*, vol. 8, no. 2, pp. 472–482, May 1993.

[29] "Standard load models for power flow and dynamic performance simulation," *IEEE Transactions on Power Systems*, vol. 10, no. 3, pp. 1302–1313, Aug 1995.

[30] K. Christakou, J. Y. Le Boudec, M. Paolone, and D. Tomozei, "Efficient computation of sensitivity coefficients of node voltages and line currents in unbalanced radial electrical distribution networks," *IEEE Transactions on Smart Grid*, vol. 4, no. 2, pp. 741–750, June 2013.

[31] DESL-EPFL, "Extension of the IEEE 39-bus Test Network for the Study of Fundamental Dynamics of Modern Power System," [Online]. Available: https://github.com/DESL-EPFL/, 2018, accessed: 2020-04-01.

[32] T. Athay, R. Podmore, and S. Virmani, "A practical method for the direct analysis of transient stability," *IEEE Transactions on Power Apparatus and Systems*, vol. PAS-98, no. 2, pp. 573–584, March 1979.

[33] Y. Zuo, G. Frigo, A. Derviškadić, and M. Paolone, "Impact of synchrophasor estimation algorithms in ROCOF-based under-frequency load-shedding," *IEEE Transactions on Power Systems*, 2019.

[34] P. Romano, M. Pignati, and M. Paolone, "Integration of an IEEE Std. C37.118 compliant PMU into a real-time simulator," in *2015 IEEE Eindhoven PowerTech*, June 2015, pp. 1–6.